

July 2022

## Computational Models to Detect Radiation in Urban Environments: An Application of Signal Processing Techniques and Neural Networks to Radiation Data Analysis

Jose Nicolas Gachancipa  
Student, gachancj@my.erau.edu

Follow this and additional works at: <https://commons.erau.edu/beyond>



Part of the [Artificial Intelligence and Robotics Commons](#), [Data Science Commons](#), [Nuclear Commons](#), [Nuclear Engineering Commons](#), [Numerical Analysis and Computation Commons](#), [Numerical Analysis and Scientific Computing Commons](#), [Other Applied Mathematics Commons](#), and the [Signal Processing Commons](#)

---

### Recommended Citation

Gachancipa, Jose Nicolas (2022) "Computational Models to Detect Radiation in Urban Environments: An Application of Signal Processing Techniques and Neural Networks to Radiation Data Analysis," *Beyond: Undergraduate Research Journal*: Vol. 6 , Article 2.

Available at: <https://commons.erau.edu/beyond/vol6/iss1/2>

This Article is brought to you for free and open access by the Journals at Scholarly Commons. It has been accepted for inclusion in Beyond: Undergraduate Research Journal by an authorized administrator of Scholarly Commons. For more information, please contact [commons@erau.edu](mailto:commons@erau.edu).

---

# Computational Models to Detect Radiation in Urban Environments: An Application of Signal Processing Techniques and Neural Networks to Radiation Data Analysis

## Cover Page Footnote

This project was supported by the Pacific Northwest National Laboratory (PNNL), who provided access to the data. I thank Dr. Mihhail Berezovski at Embry-Riddle Aeronautical University and Dr. Aaron Luttmann at PNNL for their support and technical advice throughout the project.

# *Computational Models to Detect Radiation in Urban Environments: An Application of Signal Processing Techniques and Neural Networks to Radiation Data Analysis*

Jose Nicolas Gachancipa

## **Abstract**

Radioactive sources, such as uranium-235, are nuclides that emit ionizing radiation, and which can be used to build nuclear weapons. In public areas, the presence of a radioactive nuclide can present a risk to the population, and therefore, it is imperative that threats are identified by radiological search and response teams in a timely and effective manner. In urban environments, such as densely populated cities, radioactive sources may be more difficult to detect, since background radiation produced by surrounding objects and structures (e.g., buildings, cars) can hinder the effective detection of unnatural radioactive material. This article presents a computational model to detect radioactive sources in urban environments, which uses signal processing techniques to identify radiation signatures. Moreover, the model uses artificial neural networks to identify types of radiation sources, classifying them as innocuous or harmful, and discerning between weapons-grade material and radioactive isotopes used in medical or industrial settings.

## **Introduction**

Radioactive sources are nuclides that emit ionizing radiation. Some of these sources, such as uranium-235 ( $^{235}\text{U}$ ) and plutonium-239 ( $^{239}\text{Pu}$ ), can be used to build nuclear weapons, while some others, such as caesium-137 ( $^{137}\text{Cs}$ ) and technetium-99 ( $^{99\text{m}}\text{Tc}$ ), are often used for medical or industrial applications. In public areas and events, the presence of a radioactive source can present a risk to the population, and therefore, it is imperative that threats are identified by radiological search and response teams. The purpose of this project is to build a computational model capable of detecting and characterizing radiation sources, using machine learning methods and statistical analysis. Specifically, the project explores the use of signal processing techniques and artificial neural networks for the analysis of radiation data.

The dataset used to develop and test the model was generated by the Oak Ridge National Laboratory and is composed of simulated environments containing a variety of radiological sources. The computational model detects unnatural radiation events in urban environments, which may have disastrous consequences if undetected or ignored. Moreover, the model identifies the types of radioactive sources,

classifying them as innocuous or harmful, and discerning between weapons-grade material and radioactive isotopes used in medical or industrial settings.

This project builds on previous research conducted by the Pacific Northwest National Laboratory (PNNL), a US government laboratory managed by the Department of Energy (DoE). The dataset used in the project was made publicly available in the paper “Data for training and testing radiation detection algorithms in an urban environment” (Ghawaly, et al., 2020). Moreover, some of the deep learning techniques previously implemented for radioactive isotope classification are discussed by Galib, et.al., in the paper “A comparative study of machine learning methods for automated identification of radioisotopes using NaI gamma-ray spectra” (Galib, Bhowmik, Avachat, & Lee, 2021), and by Gomez-Fernandez et.al., in the paper “Isotope identification using deep learning: An explanation” (Gomez-Fernandez, et al., 2021).

## Data and Methodology

The dataset used to build the computational model was generated by the Oak Ridge National Laboratory (ORNL) using a stochastic-simulation code based on Monte-Carlo methods, called MAVRIC. The details of the simulations used to train and test the model are explained by Ghawaly, et.al. in “Data for training and testing radiation detection algorithms in an urban environment”, the article that made the dataset publicly available. The dataset was created with a variety of simulated street models, each having a different radiological source, building layout, and building material. Moreover, the shielding of radioactive sources was modified for each simulation, so that more possible urban radiation scenarios would be covered. The six radiological sources included in the dataset are the following:

1. **Highly Enriched Uranium (HEU):** Uranium (U) is an element often found in nature in the form of the  $^{238}\text{U}$  and  $^{235}\text{U}$  isotopes.  $^{238}\text{U}$  cannot sustain a fission chain reaction, while  $^{235}\text{U}$  is the only fissile isotope which exists in nature. HEU is an enriched form of Uranium (composed of at least 20% of the  $^{235}\text{U}$  isotope) and can be used to build nuclear weapons (US Department of Energy, 2001).
2. **Weapons grade plutonium (WGpu):** Plutonium-239 ( $^{239}\text{Pu}$ ) is obtained when a uranium-238 ( $^{238}\text{U}$ ) isotope absorbs one neutron and decays, which occurs often in nuclear reactors. WGpu is composed of at least 93%  $^{239}\text{Pu}$  (Makhijani, 1997).
3. **Iodine ( $^{131}\text{I}$ ):** Iodine is often used for medical applications. Specifically, it is used to treat thyroid cancer. The  $^{131}\text{I}$  isotope is produced through fission in nuclear reactors, and it is widely abundant, cheap, and easy to create (Washington State Department of Health, 2003).

4. **Cobalt ( $^{60}\text{Co}$ ):**  $^{60}\text{Co}$  is produced artificially in nuclear reactors. Cobalt is often used in medical and industrial applications. Exposure to large amounts of  $^{60}\text{Co}$  can cause skin burns and cancer (National Center for Environmental Health (NCEH), 2018).

5. **Technetium ( $^{99m}\text{Tc}$ ):** Technetium-99 is also a product of nuclear reactors and can be found in nuclear waste.  $^{99m}\text{Tc}$  is a modified isotope of Technetium-99. The  $^{99m}\text{Tc}$  isotope has a very short life (5-6 hours) and does not remain inside human bodies for long periods of time. Hence, it is widely used for medical purposes (EPA, 2017).

6. **Highly Enriched Uranium (HEU) + Technetium ( $^{99m}\text{Tc}$ ):** A combination of sources 1 and 5.

The simulations in the dataset consisted of moving a Sodium Iodide (NaI) radiation detector along a simulated street (see Figure 1) while collecting energy data. Each simulation in the dataset contains a single radiological source. Moreover, small or moving objects (i.e., cars, people, traffic lights, etc.) were ignored and not included in the simulations. The dataset contains a total of 25,540 simulations, split between training and testing data. In this study, a subset of 4,800 simulations (800 per source) was used to train and test the models. The dataset files contain data of the frequency and strength of the radiation events. Each row in the data files is a radiation event described by two features: the time elapsed since the last photon was detected, in seconds, and the photon energy measured in kiloelectron-volts (keV). For the training data, the target time, which is the time at which the radiation detector is closest to the radioactive source, is also given.

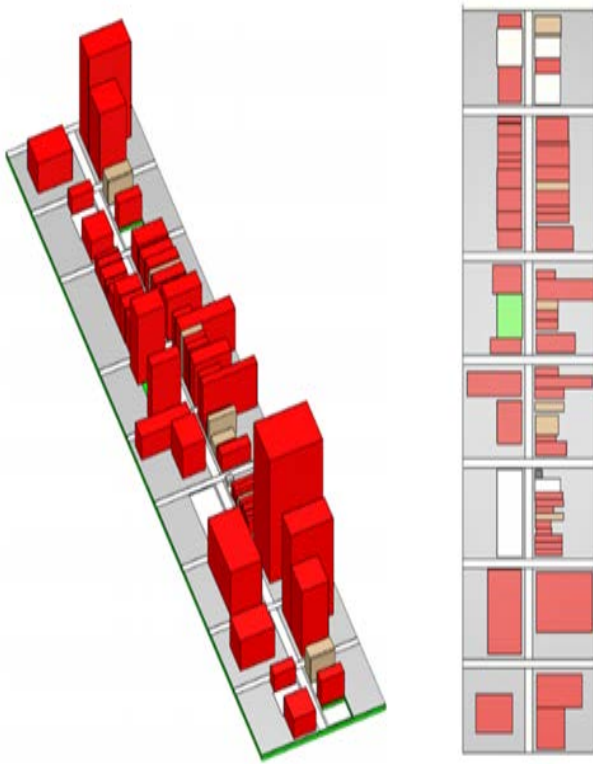


Figure 1: 3D & 2D views of a street-model comprised of brick buildings (red), granite (tan), asphalt (white), and soil (green).  
Source: (Ghawaly, et al., 2020).

The task of detecting a radioactive source from urban environment data is not trivial. Buildings and other surrounding structures produce natural background radiation, which is predominantly composed of potassium (K), uranium (U), and Thorium (T), and is commonly referred as the KUT background. Urban environments often have high levels of KUT radiation. Thus, it is difficult to differentiate radiation produced by anomalous sources from the natural (KUT) background in such environments (Anderson-Cook, et al., 2020).

Moreover, when detecting unnatural radiation, it is also important to identify the types of radiation sources, since some of these sources are harmless or do not present a significant risk. For example, from the six radiological sources included in the dataset,  $^{131}\text{I}$  and  $^{99\text{m}}\text{Tc}$  are often used for medical purposes. Therefore, it is important to recognize such sources as innocuous (at least when they are present in low quantities), so that people undergoing radiation medical treatment

are not identified as a threat by an algorithm (US Department of Energy, 2001). Furthermore, radiation detection algorithms must avoid the non-detection of harmful sources (false negatives), which can compromise the population's safety.

The goal of an urban radiation detection algorithm is to detect, identify, and locate a radiological source, while extracting KUT noise and minimizing the occurrence of false-negatives and/or false-positive alerts. This project explores two algorithms to detect and classify radioactive events, respectively. The detection algorithm utilizes signal processing methods to expose energy deviations in the data that indicate the presence of a radioactive source, while the characterization algorithm uses artificial neural networks to classify isotopes.

### 1. Radiation Detection

Signal processing is a subfield of electrical engineering focused on the analysis of data from physical events (Apolinário & Diniz, 2014). The subfield is often applied to radiation-related domains, such as medical imaging, astronomy, and radiation detection (Spieler, 2001). In this project, signal processing methods are used to detect radioactive sources based on their energy levels. Figure 2 shows the four-step process used by the model to perform radiation detection.

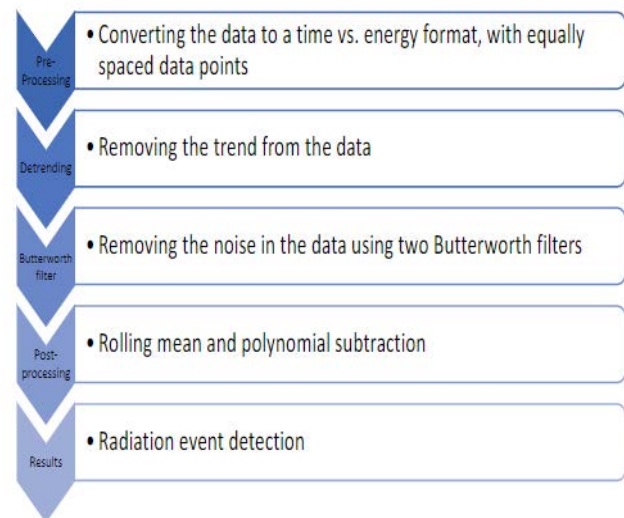


Figure 2: Radiation detection process using detrending and filtering techniques.

The first step in the proposed method is the data pre-processing step. As previously mentioned, the raw data contains the time elapsed since the last photon was detected, in seconds, and the photon energy measured in kiloelectronvolts (keV). Therefore, the raw data is an unevenly spaced time series, since the spacing between radiation events is not constant. In order to allow the signal-processing algorithm to treat the radiation data as a signal, the input data needs to be converted to a time-series with evenly spaced events. Thus, the data pre-processing stage involves finding the average photon energy detected by the NaI scintillator in each 10-millisecond time interval. The resulting dataset contains an evenly spaced time-series resembling a 100 Hz signal (100 radiation events per second, at intervals of 0.01s each).

The second step is detrending, which consists of removing the trend from the data by applying polynomial subtraction. Trends in data are usually the effect of external factors and should be removed before the analysis. For example, in datasets collected over long periods of time, detrending is often necessary to remove the seasonal/cyclical effects from the data. In the case of radiation data, detrending may be useful to remove external factors such as KUT background or the detector's built-in noise. By removing the trend from the data, it is possible to visualize strong deviations from the linear trend that may indicate the presence of an unnatural radiation source.

One of the parameters that must be defined for detrending is the order of the polynomial. In this project, the standard approach of a least-squares fitting algorithm with a 1st order polynomial is used to remove the trend from the 1000 Hz signal. Such method is visualized in Figure 3. It is important to note that once the data is detrended, the resulting energy signal is still measured in kiloelectronvolts (keV), but rather than representing the total energy collected by the radiation detector, it represents the energy-deviation from the best line of fit.

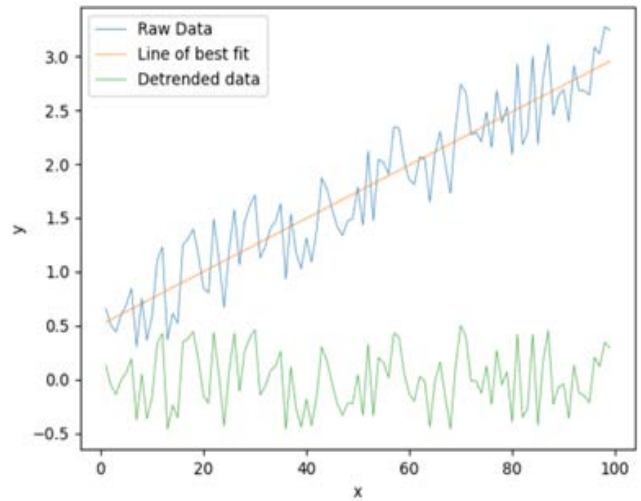


Figure 3: Example of data detrending using a first order polynomial.

Once the data is detrended, a Butterworth filter is applied to isolate frequencies in the signal, which can indicate the presence of a radioactive source such as technetium or uranium. Butterworth filters are a signal processing method to attenuate or remove frequencies that are above/below a predefined cutoff. Low-pass filters attenuate frequencies above the cutoff, while high-pass filters diminish frequencies below the defined cutoff value. For example, let us consider a 10 Hz signal superimposed over a 1 Hz frequency (see Figure 4). Upon applying a low-pass Butterworth filter with a cutoff of 5 Hz, the 10 Hz frequency is removed. Conversely, applying a high-pass Butterworth filter with the same 5 Hz cutoff would remove the 1 Hz frequency from the signal.

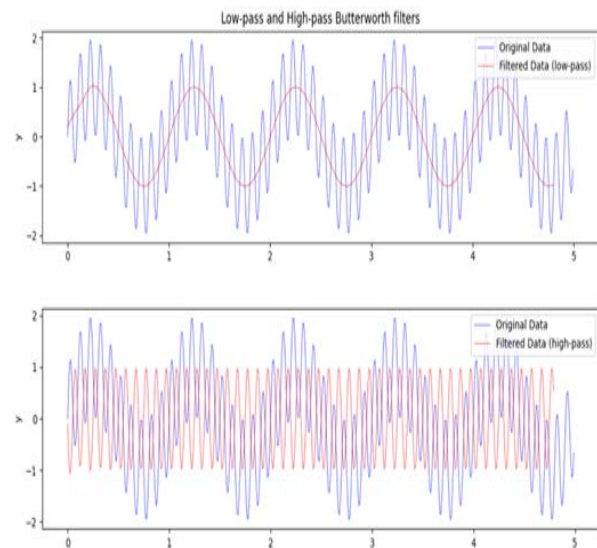


Figure 4: Overview of low-pass (top) and high-pass (bottom) Butterworth filters with a cutoff frequency of 5 Hz applied on a signal of two superimposed frequencies (1 Hz and 10 Hz).

High-pass and low-pass filters can be combined to create a Butterworth passband, which attenuates frequencies outside a specific range, rather than cutoff. For instance, in the example above, a Butterworth passband with a range between 0.5 Hz and 10 Hz would allow both frequencies to pass, since both 1 Hz and 10 Hz fall within that range, while a passband range between 0.5 Hz and 5 Hz would only remove the higher frequency (10 Hz) from the data. Furthermore, the Butterworth filter also depends on a polynomial order, which is provided as a parameter. The order defines the degree of attenuation of the frequencies that fall outside the defined cutoff or range. In general, high polynomial orders (i.e., degree 9 or 10) tend to completely remove out-of-range frequencies, while low polynomial orders (i.e., 1 or 2) attenuate those frequencies to a lesser degree. Initially, the proposed model uses a 5th order polynomial, a mid-order polynomial that attenuates frequencies outside the passband range without fully removing them. In order to use Butterworth filters, the data must be first converted from time to frequency domain, using Fourier transforms. The conversion allows the data to be analyzed by looking at the frequency distribution of the signal, rather than its behavior as a function of time. Moreover, when a signal is transformed to the frequency domain, it is possible to visualize the data in a continuous wavelet transform (CWT) plot, also known as a magnitude scalogram. The CWT is a tool used to analyze the time-varying frequency characteristics of signals (Sadowsky, 1994). In other words, the CWT displays the signal frequency and magnitude as a function of time. Figure 5 shows a CWT graph displaying the frequency distribution of a Cobalt-60 signal, through a period of 180 seconds. Note that by visualizing the CWT figure (right) it is possible to determine that the signal experienced high magnitudes between seconds 95 and 120, especially in the lower frequencies. This is not visible in the raw data (left) when the simulation is examined in the time domain.

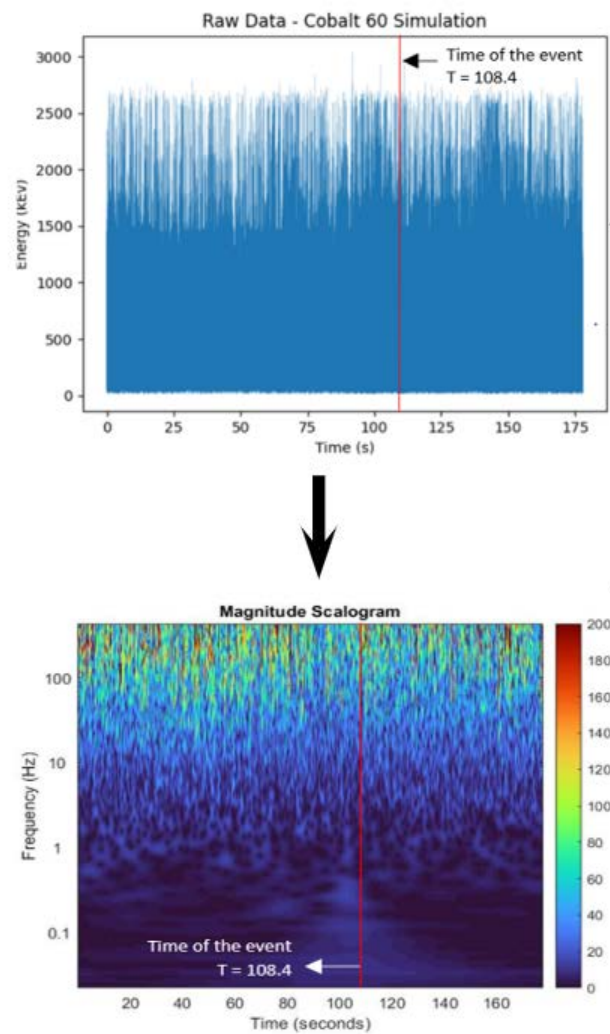


Figure 5: Raw data (top) of a Uranium-235 simulation, and its continuous wavelet transform plot (bottom). The CWT plots were generated with MATLAB's Continuous 1-D wavelet transform function.

Continuous wavelet transform plots are convenient to determine the specific frequency thresholds that define the passband range of the Butterworth filter. For example, in the CWT plot shown in Figure 5, a passband range between 0 Hz and 1 Hz would attenuate the noisy high frequencies at which the signatures of the radioactive source are not visible. Upon filtering out those frequencies, the data can be converted back to a time-domain and can be visualized in a time-energy plot.

The last step of the proposed method is to implement a simple moving average (SMA). The SMA technique is used to remove small oscillations that are not representative of the general trend of the signal and is applied mainly for data visualization purposes. The resulting plot (Figure 6) shows a noticeable energy-deviation peak at the time when the radiation detector was close to the radioactive source ( $t = 108.4s$  for the Cobalt 60 example).

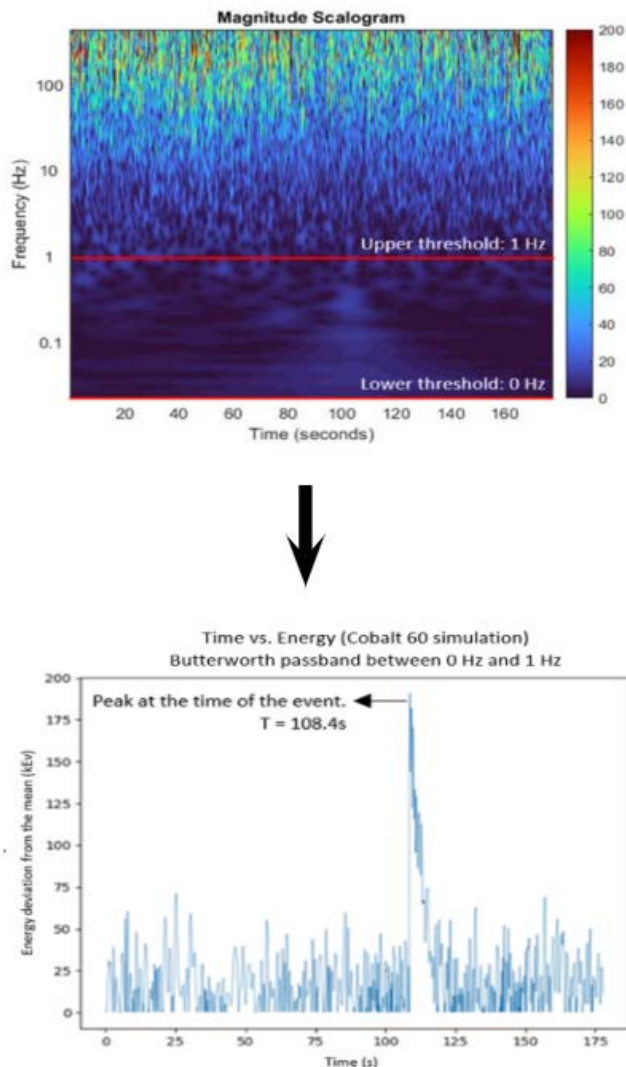


Figure 6: CWT plot with Butterworth cutoff values (top) and the resulting time vs. energy plot in the time domain (bottom) upon applying the Butterworth filter and a simple moving average (SMA).

The resulting plot can be used to identify the time at which the maximum energy deviation occurred – or detection time. Since the real time when the detector was closest to the source (target

time) is known for the simulations in the training dataset, it is possible to determine the precision of the signal processing model by comparing the detection and target times, as follows:

$$T_{\text{error}} = \text{abs}(T_{\text{target}} - T_{\text{detection}})$$

$T_{\text{error}}$  was computed for 4,800 simulations (800 simulations of each source) to determine the effectiveness of the model at detecting distinct types of radioactive sources.

## 2. Radiation characterization

Radiation detection algorithms must also be capable of identifying types of radioactive sources. The threat that each radioactive isotope poses to humans is different, and therefore, radiation detectors must discern medical/ industrial isotopes from weapons-grade material. For example,  $^{131}\text{I}$  and  $^{99\text{m}}\text{Tc}$  are often used for medical purposes, and thus, radiation detectors may indicate the presence of radiation when they are close to patients who are going through certain medical treatments, like chemotherapy. On the other hand, it is imperative for a radiation detection algorithm to identify dangerous isotopes (e.g., weapons-grade plutonium - WGPu) without failure, to avoid catastrophic consequences. The method presented in this section uses artificial neural networks to identify six types of radioactive sources from the dataset. The model uses energy spectrum data to identify features that indicate the presence of a specific radioactive isotope. The purpose of developing a deep learning model is to complement the signal processing technique previously discussed, and to enhance the detection and identification of radioactive isotopes by combining both methods.

The artificial neural network developed in this project uses energy spectrum data to classify isotopes. The energy spectrum, or gamma-ray spectrum, is one of the key distinctive features of radiological sources and it is described by the number of photons (count-rate) detected by a NaI scintillator during a time interval, as a function of

photon energy (Ghawaly, et al., 2020). For example, if the radiation device detects 40 photons with energies between 100keV and 102keV during a period of 5 seconds, the count rate for the 100-102 keV energy bin would be 8 (40 events divided by 5 seconds = 8 per second). Figure 7 shows the energy spectra of  $^{60}\text{Co}$  and  $^{235}\text{U}$ . To train the neural network, the original dataset was processed to obtain the energy spectrum of each training simulation at the time when the radiation detector was near the radiological source (target time). A window of five seconds before the target time was used to obtain the gamma-ray spectrum of each source. Moreover, the energy levels were divided into 1500 energy bins, each containing the count rate of a 2 keV range.

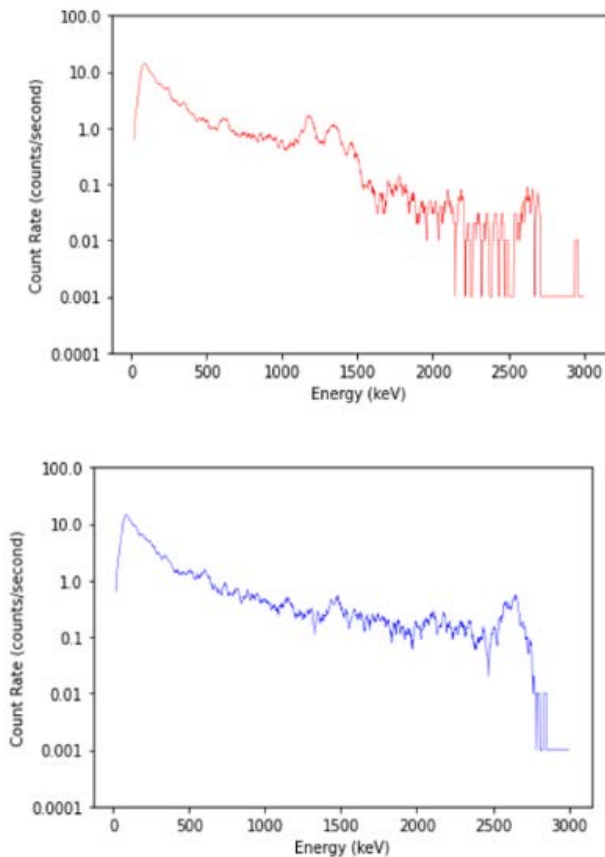


Figure 7: Energy spectrum of Cobalt-60 (top) and High Enriched Uranium-HEU (right).

The energy spectrum of radioactive sources is used for classification tasks because it contains features that are particular to each element. For example, the  $^{60}\text{Co}$  isotope is characterized for its two prominent peaks between 1000 and 1500 keV, which can be visualized in Figure 7. Neural networks use such distinctive features to discern and classify isotopes.

The neural network model created for this project was trained to identify six types of radioactive sources, using a multi-layer architecture. The network takes 1500 data points as inputs ( $x$ ), each representing the count rate of a 2 keV photon-energy bin. The weights and bias values, which are the model parameters, were obtained by training the neural network with 3,600 simulations from the dataset, which included 800 simulations of each radioactive source. The output layer of the network contains 6 neurons, each returning a probability corresponding to a specific radioactive isotope. For any given input, the output neuron returning the highest probability corresponds to the radioactive source identified by the neural network. The process is summarized in Figure 8.

Moreover, the neural network was complemented with an algorithm that generates gamma-ray spectrum data every second and delivers it to the deep learning model. Consequently, the model can be used to detect and identify radioactive isotopes on a rolling basis in continuous datasets.

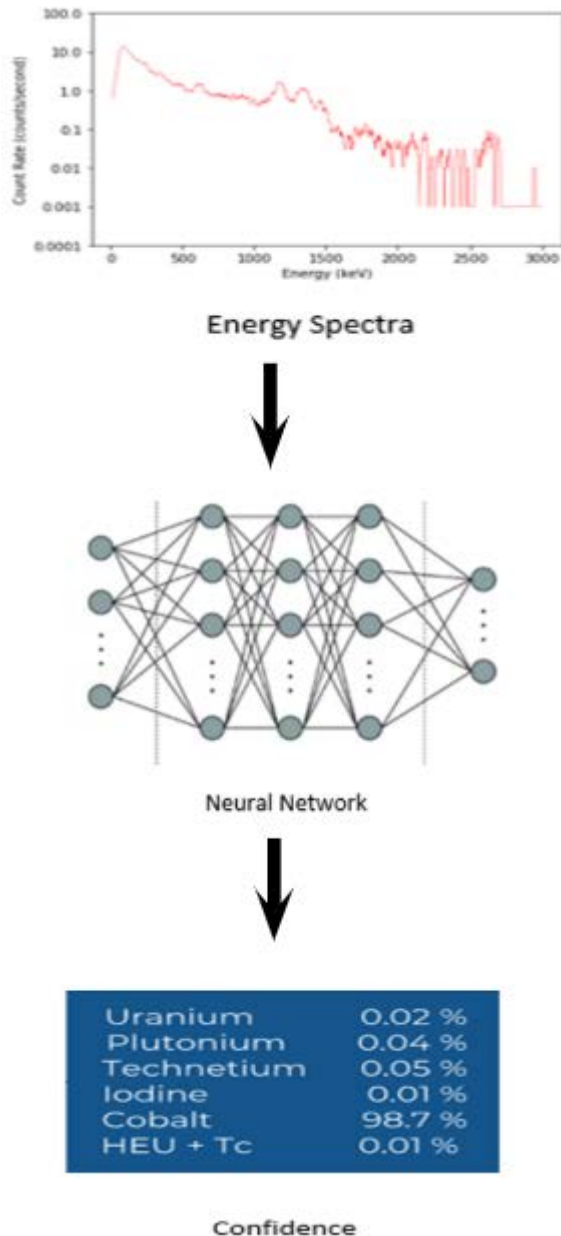


Figure 8: Radioactive source classification using an artificial neural network.

## Results

The signal processing model was tested using 4,800 simulations from the data set (800 per radioactive source). Upon processing, detrending, and filtering the data, the time difference ( $T_{error}$ ) between the model detection time and the target time (real event time) of each simulation was computed, using Equation (1). Since the goal of the signal processing model is to detect radioactive sources in a precise way, low values of  $T_{error}$  are

desired since they suggest that the model can detect radioactive sources in a timely manner. Moreover, large  $T_{error}$  values (i.e., more than 10 seconds) returned by the model indicate that the maximum energy deviation in a simulation was not observed near the target time, which implies that the radiation event was undetected by the model. Thus, simulations with  $T_{error}$  values of less than 10 seconds were denoted as “detection events”. Table 1 shows the percentage of detection events, as well as their average time error for each radioactive isotope.

Source	Simulations Tested	Detection within 10 seconds of target time (detection events)	Average $T_{error}$ (s) of detection events
Uranium	800	741 (92.6%)	1.27
Plutonium	800	488 (61.0%)	2.62
Iodine	800	429 (53.6%)	2.88
Cobalt	800	728 (91.0%)	1.09
Technetium	800	604 (75.5%)	2.01
HEU+Tech	800	714 (89.3%)	1.42
<b>Total</b>	<b>4800</b>	<b>37094 (77.2%)</b>	<b>1.88</b>

Table 1: Average time error of the model (detection time minus target time) for each radioactive isotope.

In general, the model was accurate at detecting uranium, cobalt, and technetium isotopes, with more than 75% of the simulations being detection events. Conversely, the model failed to detect strong energy deviations in plutonium and iodine simulations, with only 61% and 54% of the radiation events being detected within 10 seconds of the target time, respectively. Moreover, the results show that the precision of the model also varies with the type of radioactive source being tested. Out of the 3704 detection events, the average time error (difference between detection time and target time) was higher for plutonium and iodine than for uranium and cobalt. This indicates that the model is not only more capable of detecting uranium and cobalt but can also detect such sources more rapidly.

Another way of visualizing the results is by looking at the percentage of simulations of each isotope that had a time error ( $T_{error}$ ) of less than a particular time threshold. Figure 9 shows the percentage of simulations that were detected within 1, 2, 3, 4, 5, and 10 seconds of the target time for each of the six radioactive sources.

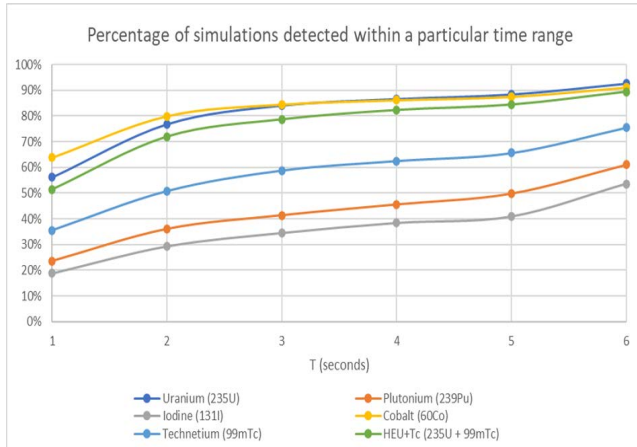


Figure 9: Radioactive events detected within a particular time (in seconds) from the target time.

Once again, Figure 9 shows that the precision of the signal processing model depends on the type of source. For instance, radiation was detected within 5 seconds of the target time in 88.4% and 87.4% of 235U and 60Co cases, respectively. Conversely, within the same time threshold, radiation was detected in only 40.9% and 49.8% of the Iodine and Plutonium simulations.

The performance of the neural network model was also evaluated. The neural network was trained using a 75-25 split of the data, using the same 4,800 simulations, 800 per radioactive source. Since the main goal of the artificial neural network is to classify radioactive isotopes, the testing algorithm focused testing if the network could find isotope signatures in gamma-ray spectra at the target time. Therefore, for testing purposes, the original simulations were reduced to include only 10 seconds of data around the target time (5 seconds before and 5 seconds after). Then, for each simulation, the neural network model was tested continuously across the 10-second interval.

The network then returned the 6 probabilities corresponding to each radioactive isotope. A confidence level of 95% was used as a threshold, meaning that if a probability corresponding to a certain isotope surpassed 95%, the neural network would alert the detection of such radioactive source. Conversely, if none of the probabilities returned by the model reached the required confidence level, the model would indicate the absence of radiation. Table 2 summarizes the results of the deep learning model in the form of a confusion matrix. As seen in the table, most of misclassified instances were either uranium or technetium events that were identified as HEU+Tech (the modified isotope that is composed of both elements).

	235U	239Pu	131I	60Co	99mTc	HEU + Tech	Undetected
Uranium (235U)	89.9%	0.0%	0.0%	0.5%	0.0%	6.50%	3.1%
Plutonium (239Pu)	0%	96.3%	0.0%	0.3%	0.0%	0%	3.4%
Iodine (131I)	0%	0%	98.6%	0.6%	0.0%	0%	0.7%
Cobalt (60Co)	0.6%	0.30%	0.0%	95.8%	0.0%	0%	3.3%
Technetium (99mTc)	0%	0.0%	0.0%	0.0%	82.1%	5.40%	12.5%
HEU + Tech	3.40%	0.0%	0.0%	0.0%	2.6%	92.7%	1.3%

Table 2: Confusion matrix- Neural network isotope classification using gamma-ray spectrum data. or see appendix 1

Finally, this study aimed to combine the signal processing and neural network models, so that they could be used complementary to detect and identify isotopes. A graphical user interface (GUI) was developed to visualize the output of both models while processing the same simulation. Figure 10 shows the output of the GUI for the 60Co simulation previously discussed, which has a target time of  $t = 108.4$  seconds.

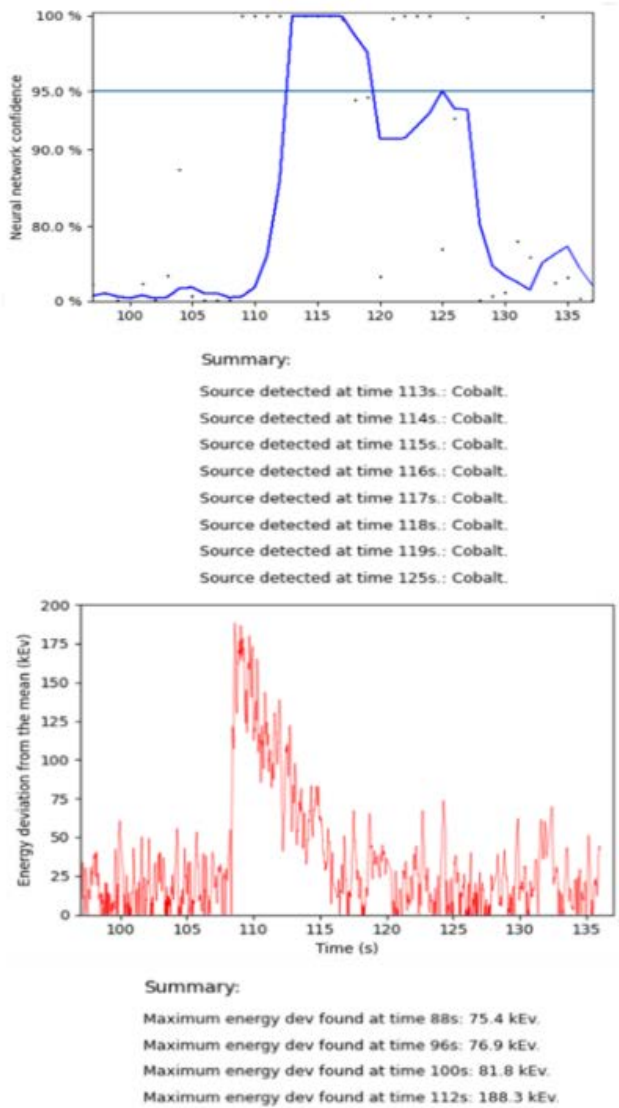


Figure 10: GUI showing the output of the neural network model (left) and signal processing algorithm (right) while processing cobalt-60 simulation with a target time of 108.4s.

The left image shows the output of the machine learning model, showing the maximum probability computed by the neural network every second. When such confidence surpasses the 95% threshold, the GUI displays the radioactive source identified by the model. Likewise, the right figure shows the output of the signal processing model, showing energy deviations as a function of time. Additionally, the model displays a note every time a new maximum energy deviation is found. For instance, in the  $^{60}\text{Co}$  sample, a maximum energy deviation was found at  $t = 112\text{s}$ , 3.6 seconds after the target time (108.4s). Similarly, the artificial neural network identified  $^{60}\text{Co}$  eight times,

between  $t=113\text{s}$  and  $t=125\text{s}$ .

## Discussion

The results of the signal processing technique show that the model's accuracy is highly dependent on the type of radioactive source. In general,  $^{235}\text{U}$ ,  $^{60}\text{Co}$  and  $^{99\text{m}}\text{Tc}$  are easier to detect than  $^{239}\text{Pu}$  and  $^{131}\text{I}$ . Likewise, the precision of the model is source-dependent since some isotopes are detected by the model in a shorter time span than others. For example,  $^{60}\text{Co}$  is detected, on average, within 1.09 seconds of the target time, while the mean detection time of  $^{131}\text{I}$  is almost 3 seconds. Since the model obtains the detection time from the maximum energy deviation (see Figure 6), it is possible that radioactive sources with low detection rates (e.g.,  $^{131}\text{I}$ ) do not generate significant deviations that can reveal the presence of radiation. Thus, further work must be undertaken to recognize the intrinsic differences between radioactive sources that lead to easier detection of certain isotopes over others, as well as to understand the physical significance of such differences.

On the other hand, it is important to note that the parameters of the Butterworth filter may be further optimized to enhance the performance of the detection algorithm. One of the parameters that can be revised is the filter's polynomial order. The proposed model uses a 5<sup>th</sup> order polynomial, which attenuates frequencies outside a passband range without fully eliminating them. The reason why a 5<sup>th</sup> order polynomial is used is that some radiation signatures may be present outside the defined passband range, and therefore, by using a mid-order polynomial, out-of-range radiation features are attenuated but not fully ignored. However, the model can be further optimized since it has not been tested with different polynomial degrees. For instance, the order can be increased to filter out more noise frequencies (Kim), with the downside that frequencies outside the passband range (which may have useful radiation signatures) will be fully removed by the filter.

Another important input parameter is the Butterworth filter's passband range, which stipulates the frequencies that are used to detect radiation signatures. The signal processing model was initially tested using a passband range between 0 Hz and 1 Hz, as shown in Figure 6. Such range was defined by visualizing a variety of simulations in the frequency domain using the continuous wavelet transform plots. The lower and upper limits of the passband range have a major impact in the precision of the algorithm, and therefore, further work must be carried out to determine the interval that provides the optimal performance. Moreover, the model could be improved by defining if distinct passband ranges could be used for different radioactive isotopes. For instance,  $^{239}\text{U}$  and  $^{60}\text{Co}$  were easily identified using a 0-1 Hz passband range and a Butterworth filter polynomial order of 5<sup>th</sup> degree. However, the performance of the model on the  $^{239}\text{Pu}$  and  $^{131}\text{I}$  isotopes may improve if different parameters are used.

On the other hand, the neural network model was highly accurate at classifying radioactive isotopes. In fact, radioactive sources were correctly characterized in 92.6% of the cases. Out of the 7.4% of the misclassified cases, almost 3% were  $^{235}\text{U}$  and  $^{99\text{m}}\text{Tc}$  simulations that were erroneously categorized in the  $^{235}\text{U} + ^{99\text{m}}\text{Tc}$  class (which is a combination of both isotopes), and vice versa. Thus, a way to enhance the performance of the neural network by 3% is to improve its ability to discern between events where a single radioactive isotope is present (e.g.,  $^{235}\text{U}$ ) from events where multiple sources are being detected by the NaI scintillator (e.g.,  $^{235}\text{U} + ^{99\text{m}}\text{Tc}$ ). Such enhancement could be feasible with more training data. Alternatively, techniques such as data augmentation could also provide more training samples without the need of running more simulations. Moreover, out of the 7.4% of misclassified events, a further 2% pertained to undetected  $^{99\text{m}}\text{Tc}$  samples. Thus, future enhancements of the neural network model should also focus on improving the ability of the model to identify signatures of the  $^{99\text{m}}\text{Tc}$  isotope from the gamma-ray spectra data.

Furthermore, a factor that may impact the performance of both models is shielding. As previously mentioned, isotopes were shielded with lead material in some simulations. A radioactive source that is shielded may be more difficult to detect and identify by an algorithm, since less gamma rays will reach the radiation scintillator, resulting in a different gamma-ray spectrum. However, the original dataset does not contain information about the level of shielding which isotopes were subject to in each specific simulation. Thus, the present study could not determine whether the signal processing and neural network model's performance was significantly different for shielded radioactive material, as compared to unshielded sources.

## Conclusion

This study presents two methods for radioactive isotope detection and identification. The first method uses signal processing techniques to remove the trend and noise from the data, and to expose energy deviations that indicate the presence of radiation. On the other hand, the machine learning model uses an artificial neural network to classify isotopes.

The study proposes the use of both methods to create an end-to-end model that can detect and identify radioactive sources in urban environments. The models were trained and tested using 4,800 simulations, which included radiation events of six different radioactive sources: uranium-235 ( $^{235}\text{U}$ ), plutonium-239 ( $^{239}\text{Pu}$ ), iodine-131 ( $^{131}\text{I}$ ), cobalt-60 ( $^{60}\text{Co}$ ), technetium-99 ( $^{99\text{m}}\text{Tc}$ ), and a combination of uranium-235 and technetium-99 ( $^{235}\text{U} + ^{99\text{m}}\text{Tc}$ ).

The signal processing model was successful at detecting certain types of radioactive isotopes, such as  $^{235}\text{U}$  and  $^{60}\text{Co}$ . However, the model did not perform well at detecting the  $^{131}\text{I}$  and  $^{239}\text{Pu}$  isotopes. Further work must be done to understand the physical differences in radioactive isotopes that may lead to a superior performance of the model at detecting certain isotopes over others. Moreover, the model can be further enhanced by tuning

the parameters of the detrending and filtering algorithms, which include the filter polynomial order, the passband range, and the detrending technique. Overall, the signal processing model detection rate was 77.2%, with most of the undetected cases corresponding to  $^{131}\text{I}$  and  $^{239}\text{Pu}$  simulations.

On the other hand, the neural network model was highly successful at characterizing radioactive sources. The model properly identified isotopes in 92.6% of the tested simulations. The performance of the model may be improved by using more training data or using a data augmentation technique. In general, the neural network's performance was limited at differentiating events with a single radioactive isotope (e.g.,  $^{235}\text{U}$ ) from those with a combination of sources (i.e.,  $^{235}\text{U} + ^{99m}\text{Tc}$ ). The model could also be further improved by knowing the shielding characteristics of each simulation, which are not provided in the original dataset.

Finally, this study proposes the integration of both models through a GUI, which shows the continuous output of the signal processing and neural network models in parallel, allowing a radiation detector to perform the detection and characterization tasks at the same time.

## References

- Anderson-Cook, C., Archer, D., Bandstra, M., Curtis, J., Ghawaly, J., Tenzing, J., . . . Quiter, B. (2020). *Radiation Detection Data Competition Report*. Los Alamos.
- Apolinário, I., & Diniz, P. (2014). *Signal Processing Theory and Machine Learning*. Rio de Janeiro, Brazil.
- Crossland, T. (2020, 07 28). *The History and Future of Neural Networks*. Retrieved from The AI Journal: <https://aijournal.com/the-history-and-future-of-neural-networks/>
- EPA. (2017, 05 23). *Radionuclide Basics: Technetium-99*. Retrieved from EPA: <https://www.epa.gov/radiation/radionuclide-basics-technetium-99>
- Galib, S., Bhowmik, P., Avachat, A., & Lee, H. (2021). A comparative study of machine learning methods for automated identification of radioisotopes using NaI gamma-ray spectra. *Nuclear Engineering and Technology*.
- Ghawaly, J., Nicholson, A., Peplow, D., Anderson-Cook, D., Myers, K., Archer, D., . . . Quiter, B. (2020). Data for training and testing radiation detection algorithms in an urban environment. *Scientific Data*.
- Gomez-Fernandez, M., Wong, W.-K., Tokuhiko, A., Welter, K., Alhawsawi, A., Yang, H., & Higley, K. (2021). Isotope identification using deep learning: An explanation. *Nuclear Inst. and Methods in Physics Research, A*.
- Kim, V. (n.d.). *How to Design 10 kHz filter. (Using Butterworth filter design)*. East Lansing, Michigan.
- Lefkowitz, M. (2019, 09 25). *Professor's perceptron paved the way for AI – 60 years too soon*. Retrieved from Cornell University: <https://news.cornell.edu/stories/2019/09/professors-perceptron-paved-way-ai-60-years-too-soon>
- Makhijani, A. (1997, 02). *Plutonium as an Energy Source*. Retrieved from IEER: <https://www.ieer.org/ensec/no-1/puuse.html>
- Muscatello, A., & Houts, M. (1996, 12 31). OSTI. Retrieved from Surplus weapons-grade plutonium: a resource for exploring and terraforming Mars: <https://www.osti.gov/biblio/459781>
- National Center for Environmental Health (NCEH). (2018, 04 04). *Radioisotope Brief: Cobalt-60 (Co-60)*. Retrieved from Center for Disease Control and Prevention (CDC): <https://www.cdc.gov/nceh/radiation/emergencies/isotopes/cobalt.htm>
- Sadowsky, J. (1994). *The continuous wavelet transform: A tool for signal investigation and understanding*. Baltimore: Johns Hopkins.
- Spieler, H. (2001). *Radiation Detectors and Signal Processing*. Heidelberg: University of Heidelberg.
- US Department of Energy. (2001). *Highly Enriched Uranium: Striking a Balance*. US Department of Energy.
- Washington State Department of Health. (2003). *Iodine-131*. Washington State Department of Health.